iScience

CellPress

Article

Positive Selection of a Serine Residue in Bat IRF3 Confers Enhanced Antiviral Protection

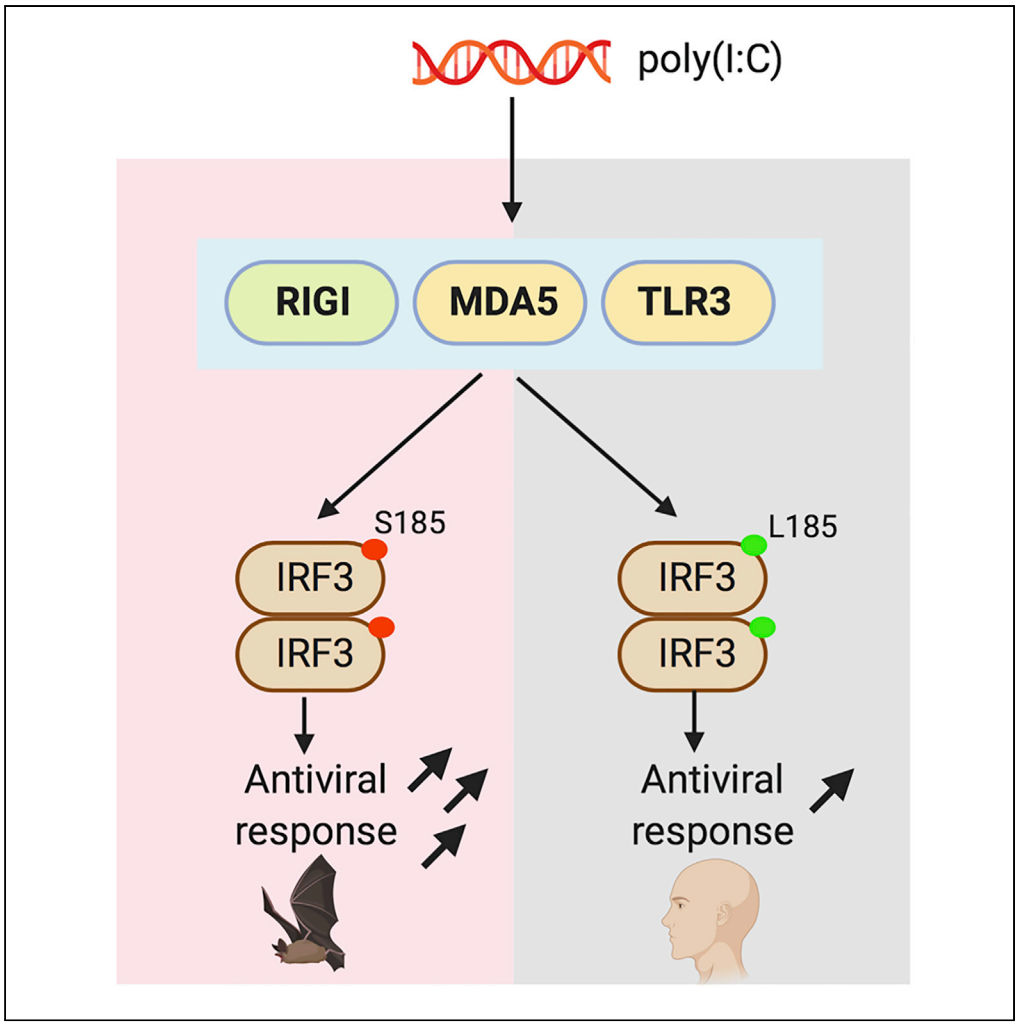

Arinjay Banerjee, Xi Zhang, Alyssa Yip, ..., Brian Golding, Lin-Fa Wang, Karen Mossman

mossk@mcmaster.ca

HIGHLIGHTS

Serine 185 is positively selected for in multiple bat IRF3 sequences

Serine 185 enhances IRF3-mediated antiviral responses in bat and human cells

IRF3-S185 function is dependent on phosphorylation

IFNAR complex is required for double-stranded RNA-mediated antiviral responses

Banerjee et al., iScience *23*, 100958
March 27, 2020
https://doi.org/10.1016/j.isci.2020.100958

iScience

CellPress

Article

Positive Selection of a Serine Residue in Bat IRF3 Confers Enhanced Antiviral Protection

Arinjay Banerjee,[1] Xi Zhang,[2] Alyssa Yip,[1] Katharina S. Schulz,[1] Aaron T. Irving,[3] Dawn Bowdish,[1] Brian Golding,[2] Lin-Fa Wang,[3] and Karen Mossman[1,4,*]

SUMMARY

Compared with other mammals, bats harbor more zoonotic viruses per species and do not demonstrate signs of disease on infection with these viruses. To counteract infections with viruses, bats have evolved enhanced mechanisms to limit virus replication and immunopathology. However, molecular and cellular drivers of antiviral responses in bats largely remain an enigma. In this study, we demonstrate that a serine residue in IRF3 is positively selected for in multiple bat species. IRF3 is a central regulator of innate antiviral responses in mammals. Replacing the serine residue in bat IRF3 with the human leucine residue decreased antiviral protection in bat cells, whereas the addition of this serine residue in human IRF3 significantly enhanced antiviral protection in human cells. Our study provides genetic and functional evidence for enhanced IRF3-mediated antiviral responses in bats and adds support to speculations that bats have positively selected for multiple adaptations in their antiviral immune responses.

INTRODUCTION

Bats are reservoirs of several emerging RNA viruses, such as filoviruses (ebolavirus and Marburg virus), paramyxoviruses (Nipah and Hendra viruses), and coronaviruses (severe acute respiratory syndrome [SARS] and Middle East respiratory syndrome [MERS] coronaviruses [CoVs]) that cause serious and often fatal disease in humans and agricultural animals (Anthony et al., 2017; Forbes et al., 2019; Ge et al., 2013; Swanepoel et al., 2007; Yang et al., 2019). More recently, SARS-CoV-2, which is causing the ongoing COVID-19 outbreak, was determined to be 96% similar at the genomic level to a bat CoV (Bat_CoV_RaTG13) that was detected in *Rhinolophus affinis* (Zhou et al., 2020). However, bats that are naturally or experimentally infected with these viruses do not demonstrate overt signs of disease (Munster et al., 2016; Hayman, 2016). These observations have led to studies that have explored innate and intrinsic antiviral immune responses in this intriguing mammalian order and the unique ability of bats to control virus infection-induced immunopathology (Pavlovich et al., 2018; Schountz et al., 2017).

In addition to identifying conserved features of the mammalian innate immune system in bats, recent studies have discovered novel adaptations in bat antiviral responses (Banerjee et al., 2020). These adaptations include constitutive expression of interferon alpha (IFNα) (Zhou et al., 2016), wider tissue distribution of interferon regulatory factor 7 (IRF7) (Zhou et al., 2014), stricter regulation of pro-inflammatory processes (Banerjee et al., 2017; Ahn et al., 2019), and atypical expression of interferon-stimulated genes (ISGs) (de La Cruz-Rivera et al., 2018; Hölzer et al., 2019). Most antiviral and innate immune signaling studies in bat cells have used surrogate virus (poly I:C, a synthetic double-stranded RNA molecule) and virus infections to stimulate downstream expression of IFNs and ISGs; however, the evolution and function of critical transcription factors, such as IRFs, and associated downstream antiviral signaling events remain an enigma.

IRF3 is a central transcription factor, and multiple antiviral signaling pathways converge on this molecule (Honda and Taniguchi, 2006; Honda et al., 2006). On sensing viral nucleic acids, pattern recognition receptors (PRRs) activate downstream signaling mediators, such as cellular kinases TANK binding kinase 1 (TBK1) and inhibitor of nuclear factor kappa-B kinase subunit epsilon (IKKε). Activated kinases phosphorylate serine residues in human IRF3 at positions 385, 386, 396, 398, and 402 to activate IRF3 (Panne et al., 2007). Activated IRF3 dimerizes and localizes to the nucleus of the cell to induce the expression of type I IFNs and downstream ISGs that induce an antiviral state in infected (autocrine) and neighboring (paracrine) cells (Kawai and Akira, 2006). A recent study in *Eptesicus fuscus* (big brown bat) cells demonstrated that IRF3 is essential for double-stranded (ds) RNA (polyI:C) and MERS-CoV infection-mediated stimulation of antiviral signaling pathways (Banerjee et al., 2019). However, residues important for IRF3 activation in bats have not been characterized. Considering the apparent asymptomatic co-existence of RNA viruses

[1]Michael DeGroote Institute for Infectious Disease Research, McMaster Immunology Research Centre, Department of Pathology and Molecular Medicine, McMaster University, Hamilton, ON L8S 4K1, Canada

[2]Department of Biology, McMaster University, Hamilton, ON L8S 4K1, Canada

[3]Programme in Emerging Infectious Disease, Duke-NUS Medical School, Singapore 169857, Singapore

[4]Lead Contact

*Correspondence: mossk@mcmaster.ca

https://doi.org/10.1016/j.isci.2020.100958

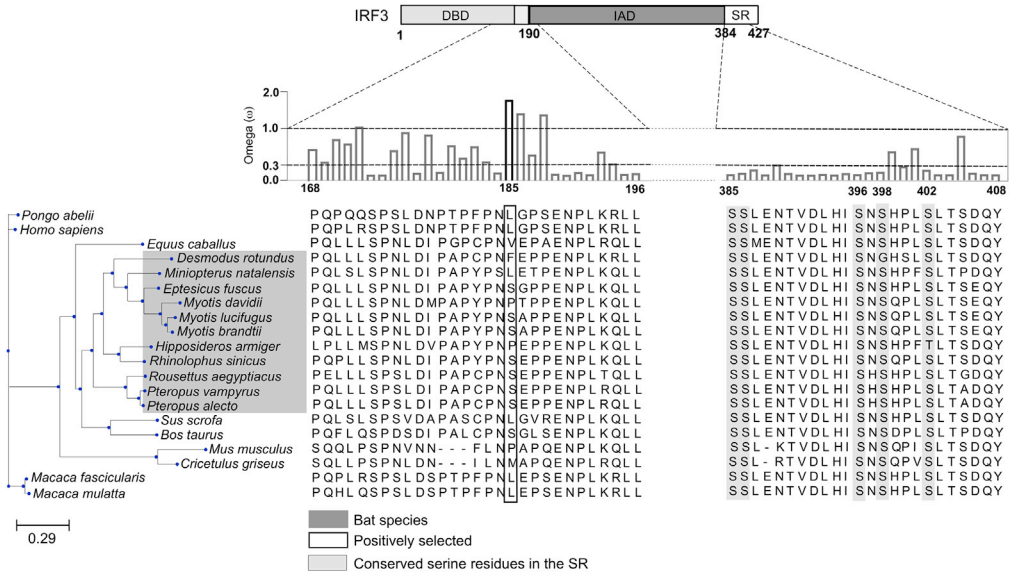

Figure 1. Positive Selection of Amino Acid Residue at the 185th Position in bat IRF3

Functional domains of IRF3 are shown in the top panel above the alignment. The ratio of non-synonymous and synonymous amino acid substitutions is denoted by the omega value. Black bar indicates significant positive selection. Bat species are highlighted in dark gray. Conserved serine residues involved in human IRF3 activation are highlighted in light gray. The 185th amino acid residue in the multiple sequence alignment is highlighted by the box. DBD, DNA-binding domain; IAD, IRF association domain; SR, serine-rich region. See also Figure S1 for details on computational analysis and Table S2 for accession numbers of IRF3 sequences.

and bats (Maxmen, 2017; Wong et al., 2019), it is important to study the evolution of RNA virus detection and subsequent antiviral signaling in this mammalian order. Bats evolved/diverged from land mammals over 80 million years ago (Teeling et al., 2005; Simmons et al., 2008), and the prolonged arms race with some of these viruses, coupled with the unique ability to fly, have likely shaped their antiviral responses (O'shea et al., 2014; Zhang et al., 2013). Considering the important role of IRF3 in mediating downstream antiviral signaling events and the ability of multiple bat-borne RNA viruses to inhibit IRF3 activation in human cells (Lui et al., 2016; Ding et al., 2014; Chen et al., 2014), bats have likely evolved sophisticated mechanisms of IRF3 activation to mount a robust antiviral response to low levels of infection.

In light of these discoveries and speculations, we hypothesized that co-existence with RNA viruses has imposed strong selective pressures on bat antiviral signaling molecules, resulting in robust antiviral responses to virus infection or immune activation signals. Since IRF3 is a key transcription factor in several virus-sensing pathways, we conducted computational and functional analyses of bat IRF3 across both sub-orders of bats, *Yinpterochiroptera* and *Yangochiroptera*. Sequence alignment of representative mammalian IRF3 sequences showed that serine (S) residues in the C-terminal serine-rich region are highly conserved (Figure 1). On performing further *in silico* analysis of IRF3 amino acid sequences, we identified that the amino acid residue at the 185th position was positively selected for in multiple bat IRF3 sequences (Figure 1). Since serine residues play a major role in IRF3 activation (Panne et al., 2007), we studied the functional importance of the serine residue at the 185th position (S185) in 7 of 11 bat IRF3 sequences.

RESULTS

Serine 185 Is Positively Selected for in Multiple Bat Species

We conducted computational and functional analyses of bat IRF3 across both suborders of bats, *Yinpterochiroptera* and *Yangochiroptera*. Sequence alignment of representative mammalian IRF3 sequences showed that serine (S) residues in the C-terminal serine-rich region are highly conserved (Figure 1). On performing further *in silico* analysis of IRF3 amino acid sequences, we identified that the amino acid residue at the 185th position was positively selected for in multiple bat IRF3 sequences (Figure 1). Since serine residues play a major role in IRF3 activation (Panne et al., 2007), we next studied the functional importance of the serine residue at the 185th position (S185) in 7 of 11 bat IRF3 sequences.

IRF3-S185 Induces a Robust Antiviral Response in Bat Cells from Two Suborders

To determine whether IRF3 is more competent in inducing robust antiviral protection due to the presence of S185, we compared the differences in antiviral response to surrogate virus infection [poly(I:C) stimulation] in bat and human cells expressing bat (S185) or human (L185) forms of IRF3, respectively. We generated *E. fuscus* and *P. alecto* wild-type (Ef IRF3-WT and Pa IRF3-WT) and altered (Ef IRF3-L185 and Pa IRF3-L185) IRF3 expression plasmids. We also generated wild-type (hu IRF3-WT) and altered (hu IRF3-S185) human IRF3 expression plasmids to determine if introducing S185 would enhance antiviral protection in human cells. To quantify the antiviral response in cells expressing wild-type or altered forms of IRF3, we performed bioassays using vesicular stomatitis virus (VSV) that was genetically engineered to express green fluorescent protein (VSV-GFP). VSV is known to infect cells from multiple species of mammals (Johannsdottir et al., 2009) and is very sensitive to IFN signaling, making it ideal for antiviral studies in cells from diverse mammalian species. In this study, we used *IRF3* deleted human fibroblast cells (THF-IRF3 KO cells) (Sali et al., 2015) and *IRF3* deleted kidney cells from two distantly related bat species, *E. fuscus* (*Yangochiroptera;* cr3-8 cells) (Banerjee et al., 2019) and *Pteropus alecto* (*Yinpterochiroptera;* PakiT03-4G cells). The use of IRF3-null cells allowed us to ectopically express wild-type and altered forms of IRF3 in a dose-dependent manner (Figure 2A).

To determine whether Ef IRF3-WT (S185) and Ef IRF3-L185 differed in their potential to activate antiviral signaling in *E. fuscus IRF3* deleted cr3-8 cells, we introduced increasing amounts of IRF3 expression plasmids in these cells (Figure 2B). We compared the extent of virus replication in Ef IRF3-WT and Ef IRF3-L185 expressing cr3-8 cells by quantifying the amount of GFP expressed by replicating VSV-GFP. Cr3-8 cells that expressed Ef IRF3-L185 displayed reduced antiviral protection compared with Ef IRF3-WT, both in the absence and presence of poly(I:C) stimulation (Figure 2B). Thus, replacing S185 with L185 in *E. fuscus* IRF3 significantly reduced poly(I:C)-induced antiviral protection in cr3-8 cells and led to higher levels of virus replication.

To determine if S185 in IRF3 was equally important for antiviral responses in a distantly related fruit bat, *P. alecto* (Figure 1), we expressed *P. alecto* WT (Pa IRF3-WT; S185) and altered (Pa IRF3-L185) IRF3 in *IRF3* deleted PakiT03-4G cells. Similar to what we observed in cr3-8 cells, expressing Pa IRF3-L185 in PakiT03-4G cells significantly reduced antiviral protection in these cells, relative to cells that expressed Pa IRF3-WT (Figure 2C). Thus, the presence of S185 in *E. fuscus* and *P. alecto* IRF3 is critical for a robust antiviral response in cells from these bats.

Introducing S185 in Human IRF3 Enhances Antiviral Responses in Human Cells

To determine whether introducing a similar serine residue in human IRF3 could enhance antiviral responses in human cells, we introduced a complementary mutation in human IRF3 by replacing L185 with S185. We expressed wild-type (hu IRF3-WT; L185) and altered (hu IRF3-S185) human IRF3 in *IRF3* deleted human (THF-IRF3 KO) cells (Figure 2D). THF-IRF3 KO cells expressing hu IRF3-S185 were better protected against VSV-GFP in the absence or presence of poly(I:C) stimulation, compared with cells that expressed hu IRF3-WT (Figure 2D). Thus, introducing a serine residue at the 185th position in human IRF3 significantly enhanced antiviral protection in human cells.

IRF3-D185 Retains Enhanced Antiviral Signaling in Stimulated Bat and Human Cells

Phosphorylation of serine residues in the C-terminal serine-rich region is known to regulate IRF3 activation in human cells (Panne et al., 2007). We next determined if the role of S185 in enhancing IRF3-mediated antiviral protection was dependent on phosphorylation. Since anti-phospho antibodies to S185 are not available, we substituted the serine residue at the 185th position with aspartate (S185D mutation) in human and bat IRF3. Aspartate mimics the charge on a phosphorylated serine residue and has been used to study cellular functions that are modulated by phosphorylated serine residues in proteins (Leger et al., 1997). We repeated our bioassays and compared antiviral responses in cells expressing L185, S185 and D185 forms of IRF3. Indeed, human and bat IRF3-D185 conferred enhanced antiviral protection in human and bat cells, respectively, relative to IRF3-L185, suggesting that the activity of S185 is dependent on a charge that is similar to a phosphorylated serine residue (Figures 3A–3C). Interestingly, IRF3-D185 conferred enhanced protection in PakiT03-4G cells, relative to IRF3-S185-expressing cells that were stimulated with poly(I:C) (Figure 3B). Similarly, IRF3-D185 expressing THF-IRF3 KO cells were better protected from VSV-GFP, relative to IRF3-S185-expressing cells (Figure 3C; mock). Transfecting 50 ng of IRF3-D185-expressing plasmid also conferred better protection in THF-IRF3 KO cells than IRF3-S185 in the presence

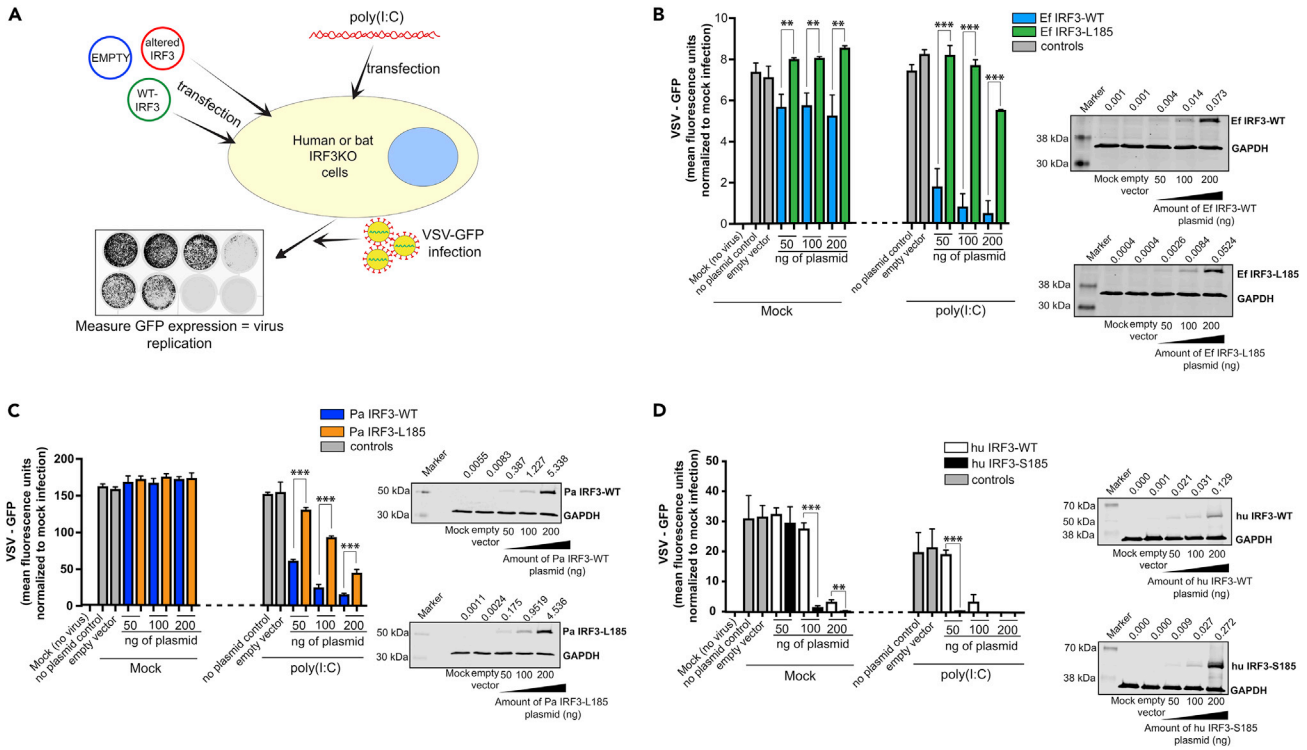

Figure 2. Human and Bat Cells Expressing IRF3-S185 Display Enhanced Antiviral Protection

(A) Schematic representation of the experimental strategy. *IRF3* knockout (KO) bat and human cells were transfected with varying concentrations of wild-type (WT) or altered IRF3 expression plasmids for 24 h. The cells were then stimulated with poly(I:C) for 6 h, followed by infection with vesicular stomatitis virus (VSV) that was engineered to express green fluorescent protein (GFP). Nineteen hours after infection, GFP expression was measured as a surrogate for virus replication.

(B) VSV-GFP replication in *E. fuscus IRF3* KO kidney cells (cr3-8) transfected with varying concentrations of plasmids expressing WT (S185) or altered (L185) *E. fuscus* IRF3 and mock treated or treated with poly(I:C) (n = 3). No plasmid and 200 ng of empty vector were used as transfection controls. Immunoblots: IRF3 protein levels in cr3-8 cells mock transfected, transfected with 200 ng empty vector (pcDNA), or transfected with varying concentrations of WT (S185) or altered (L185) IRF3 expression plasmids.

(C) VSV-GFP replication in *P. alecto IRF3* KO kidney cells (PakiT03-4G) transfected with varying concentrations of plasmids expressing WT (S185) or altered (L185) *P. alecto* IRF3 and mock treated or treated with poly(I:C) (n = 3). No plasmid and 200 ng of empty vector were used as transfection controls. Immunoblots: IRF3 protein levels in PakiT03-4G cells mock transfected, transfected with 200 ng empty vector (pcDNA) or transfected with varying concentrations of WT (S185) or altered (L185) IRF3 expression plasmids.

(D) VSV-GFP replication in human *IRF3* KO cells (THF-IRF3-KO) transfected with varying concentrations of plasmids expressing WT (L185) or altered (S185) human IRF3 and mock treated or treated with poly(I:C) (n = 3). No plasmid and 200 ng of empty vector were used as transfection controls. Immunoblots: IRF3 protein levels in THF IRF3 KO cells mock transfected, transfected with 200 ng empty vector (pcDNA) or transfected with varying concentrations of WT (L185) or altered (S185) IRF3 expression plasmids.

Data are represented as mean ± SD, n = 3, $^{**}p < 0.01$, $^{***}p < 0.001$ (Student's t test). GFP expression is represented after normalization with mock infected cells. IRF3 protein expression and quantification data are expressed as a ratio of IRF3/GAPDH levels on top of the blots. Blots were quantified using Image Studio (LI-COR) (n = 3). KO, knockout; WT, wild-type; Ef, *E. fuscus*; Pa, *P. alecto*; Hu, human; NS, not significant.

of poly(I:C) stimulation (Figure 3C). However, in the presence of poly(I:C), 100 ng of plasmid transfection of D185 and S185 forms of human IRF3 conferred comparable and significant protection in THF-IRF3 KO cells, relative to IRF3-L185 (Figure 3C). There were no significant differences in antiviral protection between S185 and D185 forms of IRF3 in cr3-8 cells (Figure 3A).

To further confirm if phosphorylation is critical for the activity of IRF3-S185, we used a human kinase inhibitor to block TBK1 and IKKε in cells expressing IRF3-S185 (Reilly et al., 2013; Yu et al., 2015). To determine if IRF3-S185-mediated antiviral responses in bat cells were dependent on TBK1 and IKKε-mediated phosphorylation, we first validated the cross-reactivity of the inhibitor in wild-type *E. fuscus* (Efk3B) and *P. alecto* (PakiT03) cells. We treated Efk3B and PakiT03 cells with varying concentrations of the inhibitor and stimulated the cells with poly(I:C) for 3 h. We used a cross-reactive phospho-IRF3 S396 antibody to detect phosphorylation of IRF3 (see Figure S1A). The inhibitor blocked phosphorylation of the 396th serine residue, a marker of IRF3

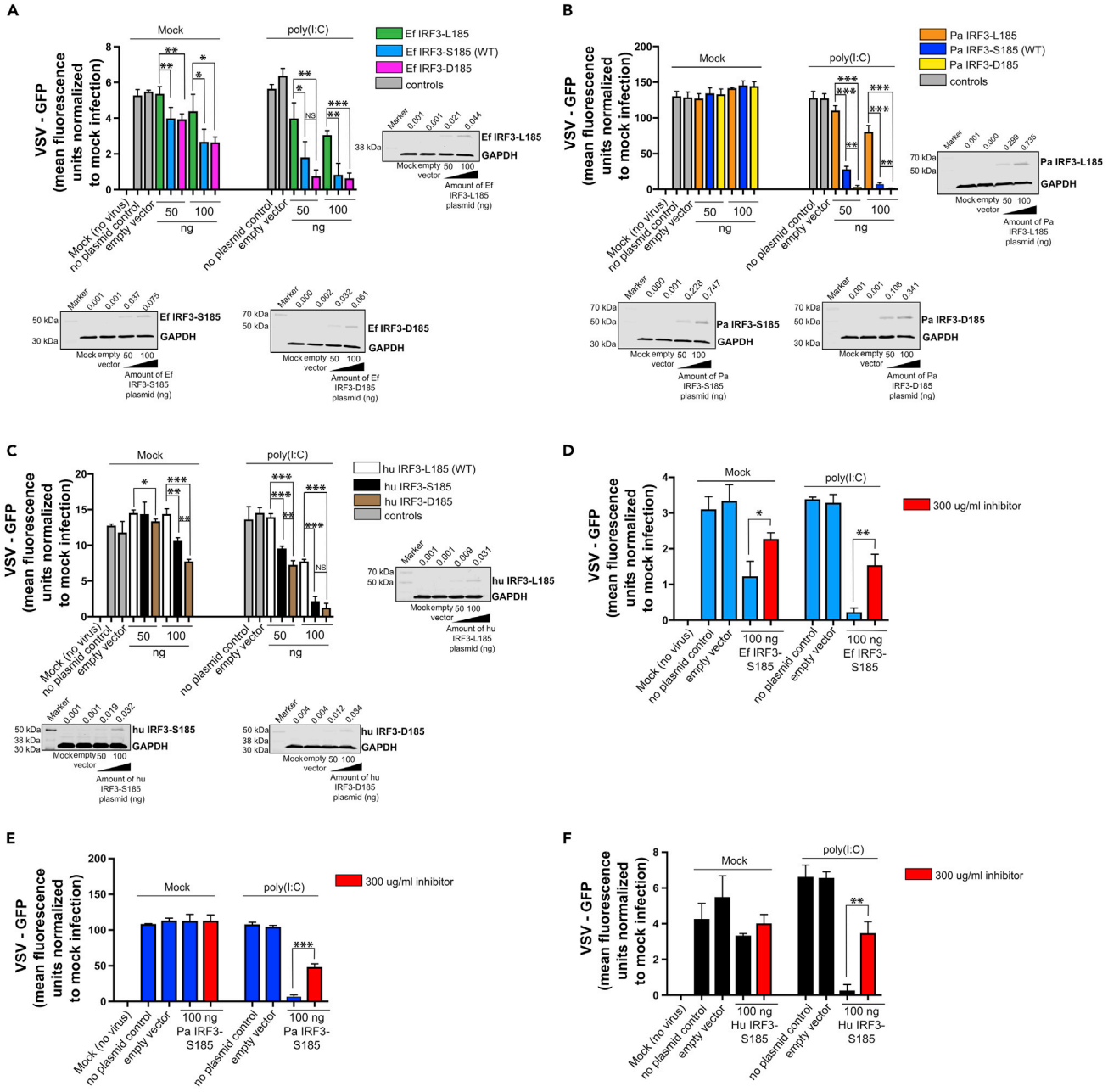

Figure 3. IRF3 S185- and D185-Expressing Bat and Human Cells Mount a Robust Antiviral Response to Double-Stranded RNA

(A) VSV-GFP replication in *E. fuscus IRF3* KO kidney cells (cr3-8) transfected with varying concentrations of plasmids expressing L185, S185, or D185 forms of *E. fuscus* IRF3 and mock treated or treated with poly(I:C) (n = 3). No plasmid and 100 ng of empty vector were used as transfection controls. Immunoblots: IRF3 protein levels in cr3-8 cells mock transfected, transfected with 100 ng empty vector (pcDNA), or transfected with varying concentrations of L185, S185, and D185 IRF3 expression plasmids.

(B) VSV-GFP replication in *P. alecto IRF3* KO kidney cells (PakiT03-4G) transfected with varying concentrations of plasmids expressing L185, S185, or D185 forms of *P. alecto* IRF3 and mock treated or treated with poly(I:C) (n = 3). No plasmid and 100 ng of empty vector were used as transfection controls. Immunoblots: IRF3 protein levels in PakiT03-4G cells mock transfected, transfected with 100 ng empty vector (pcDNA), or transfected with varying concentrations of L185, S185, or D185 IRF3 expression plasmids.

(C) VSV-GFP replication in human *IRF3* KO cells (THF-IRF3-KO) transfected with varying concentrations of plasmids expressing L185, S185, or D185 forms of human IRF3 and mock treated or treated with poly(I:C) (n = 3). No plasmid and 100 ng of empty vector were used as transfection controls. Immunoblots: IRF3 protein levels in THF-IRF3-KO cells mock transfected, transfected with 100 ng empty vector (pcDNA), or transfected with varying concentrations of L185, S185, and D185 IRF3 expression plasmids.

Figure 3. *Continued*

(D) VSV-GFP replication in *E. fuscus IRF3* KO kidney cells (cr3-8) transfected with 100 ng of plasmid expressing *E. fuscus* IRF3-S185 and mock treated or treated with 300 μg/mL of TBK1 and IKKε inhibitor. After treatment with the inhibitor, cells were mock stimulated or stimulated with poly(I:C) (n = 3). Normalized VSV-GFP levels in cells treated with TBK1 and IKKε inhibitor are denoted by red bars. No plasmid and 100 ng of empty vector were used as transfection controls.

(E) VSV-GFP replication in *P. alecto IRF3* KO kidney cells (PakiT03-4G) transfected with 100 ng of plasmid expressing *P. alecto* IRF3-S185 and mock treated or treated with 300 μg/mL of TBK1 and IKKε inhibitor. After treatment with the inhibitor, cells were mock stimulated or stimulated with poly(I:C) (n = 3). Normalized VSV-GFP levels in cells treated with TBK1 and IKKε inhibitor are denoted by red bars. No plasmid and 100 ng of empty vector were used as transfection controls.

(F) VSV-GFP replication in human *IRF3* KO cells (THF-IRF3-KO) transfected with 100 ng of plasmid expressing human IRF3-S185 and mock treated or treated with 300 μg/mL of TBK1 and IKKε inhibitor. After treatment with the inhibitor, cells were mock stimulated or stimulated with poly(I:C) (n = 3). Normalized VSV-GFP levels in cells treated with TBK1 and IKKε inhibitor are denoted by red bars. No plasmid and 100 ng of empty vector were used as transfection controls.

Data are represented as mean ± SD, n = 3, *$p < 0.05$, **$p < 0.01$, ***$p < 0.001$ (Student's t test). GFP expression is represented after normalization with mock infected cells. IRF3 protein expression and quantification data are expressed as a ratio of IRF3/GAPDH levels on top of the blots. Blots were quantified using Image Studio (LI-COR) (n = 3). KO, knockout; WT, wild-type; Ef, *E. fuscus*; Pa, *P. alecto*; Hu, human; NS, not significant. See also Figure S1.

activation, in cells from both species of bats in response to poly(I:C) stimulation (see Figures S1B and S1C). Next, we tested the effect of using the inhibitor in *IRF3* deleted bat cells expressing IRF3-S185. Ef and Pa IRF3-S185-expressing bat cells (cr3-8 and PakiT03-4G cells, respectively) that were treated with the inhibitor and stimulated with poly(I:C) had significantly higher levels of virus replication, relative to mock inhibitor-treated and poly(I:C)-induced IRF3-S185-expressing cells (Figures 3D and 3E). For cr3-8 cells expressing IRF3-S185, treating the cells with the inhibitor reduced basal levels of antiviral protection even in the absence of poly(I:C) (Figure 3D; mock). As observed in bat cells, inhibiting TBK1 and IKKε in THF-IRF3 KO cells expressing human IRF3-S185 significantly increased virus replication (Figure 3F).

Wild-Type and IRF3-S185-Mediated Antiviral Responses in Bat and Human Cells Are Dependent on IFNAR Complex

Activation of IRF3 following an exogenous stimulus induces the expression of type I IFNs (Honda et al., 2006) and the subsequent expression of antiviral ISGs via binding to the IFN α/β receptors 1 and 2 complex (IFNAR1 and IFNAR2) (de Weerd et al., 2007). We and others have also shown that IRF3-mediated signaling can induce ISG expression independent of IFN production (Ashley et al., 2019; Noyce et al., 2011). To determine if antiviral protection observed in cells expressing S185 or L185 forms of IRF3 was dependent on type I IFN signaling, we repeated our bioassays (Figure 2A) in *IRF3* and *IFNAR1* double knockout (dKO) human cells (THF-IRF3-IFNAR1 dKO) and *IRF3* and *IFNAR2* dKO *P. alecto* (PakiT03-IFNAR2-IRF3-G6) cells. Expressing hu IRF3-WT (L185) or hu IRF3-S185 in THF dKO cells (Figure 4B) did not induce antiviral protection upon poly(I:C) stimulation (Figure 4A). Similarly, expressing Pa IRF3-WT (S185) or Pa IRF3-L185 in PakiT03-IFNAR2-IRF3-G6 dKO cells (Figure 4D) did not induce antiviral protection in response to poly(I:C) (Figure 4C). These data demonstrate that IRF3-L185 and S185-mediated antiviral responses to double-stranded RNA in human and bat cells are dependent on canonical IFN signaling via the IFNAR complex. The lack of antiviral protection in *IRF3* and *IFNAR* deleted human and bat cells demonstrate that antiviral protection in our bioassays are mediated through type I IFNs (Uzé et al., 1990).

DISCUSSION

Bats harbor many zoonotic RNA viruses and do not demonstrate signs of disease when they are naturally or experimentally infected with these viruses (Munster et al., 2016; Schuh et al., 2017; Amman et al., 2015). Multiple studies have demonstrated the ability of bat cells to produce antiviral IFNs and downstream ISGs; however, the role of key transcription factors, such as IRF3 in the antiviral signaling cascade has not been studied. In this study, we provide genetic and functional evidence that multiple bat IRF3 sequences have positively selected for a serine residue that confers enhanced antiviral protection in both bat and human cells. Interestingly, we also observed that *Desmodus rotundus* IRF3 sequence contained a phenylalanine residue at the 185th position and a glycine residue at the 398th position (Figure 1) and *Hipposideros armiger* IRF3 sequence contained a proline residue at the 185th position and a threonine residue at the 402nd position (Figure 1). As high-quality sequences and cell lines from these bats become available, it will be interesting to test the functional relevance of these mutations in bat IRF3 at the 185th position and the serine-rich region.

We observed a decrease in the antiviral response in unstimulated *E. fuscus* (cr3-8) cells expressing IRF3-L185 (Figure 2B). These data suggest that S185 in bat IRF3 may contribute to higher basal levels of IFNs and associated antiviral protection in bat cells, as reported by Zhou et al. (2016). However, we did not observe an obvious similar

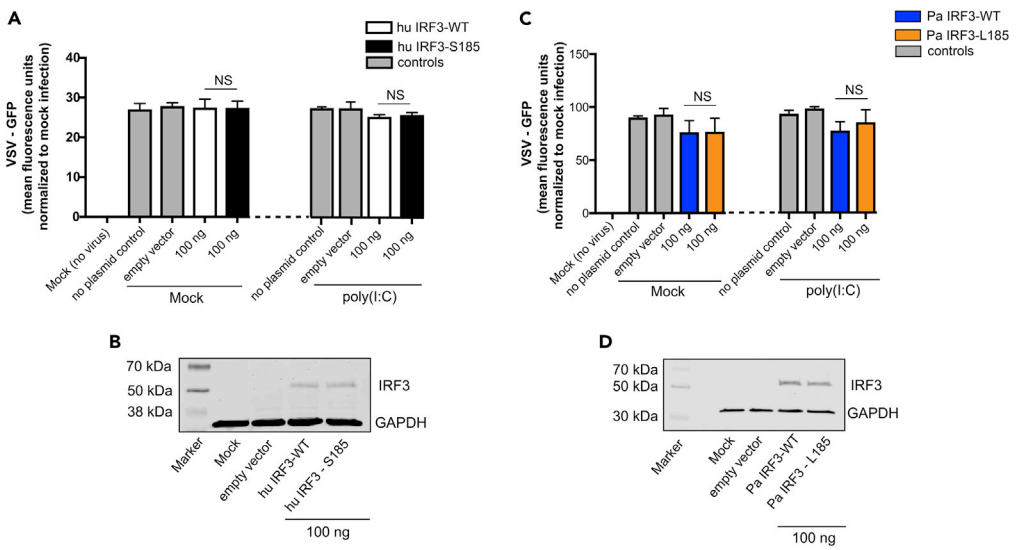

Figure 4. Wild-Type IRF3 and IRF3-S185-Mediated Antiviral Responses in Bat and Human Cells Are Dependent on the Expression of the IFNAR Complex

(A) VSV-GFP replication in human *IRF3* and *IFNAR1* (THF-IRF3-IFNAR1 dKO) deleted cells transfected with 100 ng of plasmid expressing WT (L185) or altered (S185) human IRF3 and mock treated or treated with poly(I:C) (n = 3). No plasmid or 100 ng of empty plasmid (pcDNA) were used as transfection controls.

(B) IRF3 expression in human *IRF3* and *IFNAR1* double knockout (THF-IRF3-IFNAR1 dKO) cells mock transfected, transfected with 100 ng empty vector (pcDNA), or transfected with 100 ng of WT (L185) or altered (S185) IRF3 expression plasmids.

(C) VSV-GFP replication in *P. alecto IRF3* and *IFNAR2* (PakiT03-IFNAR2-IRF3-G6 dKO) deleted cells transfected with 100 ng of plasmid expressing WT (S185) or altered (L185) *P. alecto* IRF3 and mock treated or treated with poly(I:C) (n = 3). No plasmid or 100 ng of empty plasmid (pcDNA) were used as transfection controls.

(D) IRF3 expression in *P. alecto IRF3* and *IFNAR2* double knockout (PakiT03-IFNAR2-IRF3-G6 dKO) cells mock transfected, transfected with 100 ng empty vector (pcDNA), or transfected with 100 ng of WT (S185) or altered (L185) IRF3 expression plasmids. Data are represented as mean ± SD, n = 3. GFP expression is represented after normalization with mock infected cells. KO, knockout; WT, wild-type; Ef, *E. fuscus*; Pa, *P. alecto*; Hu, human; NS, not significant.

response in unstimulated *P. alecto* cells (Figure 2C), highlighting the species diversity of bats (Teeling et al., 2005) and differences in cell types cultured from bats. In addition, we also observed that transfecting increasing concentrations of the IRF3 expression plasmid, in the absence of poly(I:C) stimulation (mock treated), did not induce strong antiviral protection in bat cells, unlike in unstimulated THF-IRF3 KO cells that were protected by higher concentrations of transfected plasmid alone (Figures 2B–2D). This observation is consistent with the recent finding that bats have evolved dampened DNA sensing and stimulator of IFN genes (STING)-mediated signaling to limit innate and intrinsic responses to self-DNA (Xie et al., 2018).

We observed that D185 form of IRF3 induced enhanced antiviral protection in response to poly(I:C) in PakiT03-4G cells, relative to S185 and L185 forms of IRF3 (Figure 3B). We observed a similar enhanced antiviral response in THF-IRF3 KO cells that were transfected with 50 ng of D185 [poly(I:C) stimulated] and 100 ng of D185 (mock stimulated), relative to cells transfected with similar concentrations of L185 and S185 IRF3 expression plasmids (Figure 3C). These data indicate that under certain circumstances, IRF3-D185 provides added antiviral protection from VSV, relative to L185 and S185 forms of IRF3. We speculate that D185 may aid in the phosphorylation of additional serine residues in the serine-rich region of IRF3 to enhance downstream antiviral responses. However, we did not observe a significant difference between S185 and D185 forms of IRF3 in cr3-8 cells (Figure 3A). Thus, although the data suggest that IRF3-D185 enhances antiviral response in human and *P. alecto* cells, relative to IRF3-S185, differences in IRF3 activation mechanisms may exist between different bat species.

Our data show that S185 enhances IRF3-mediated antiviral responses in human and bat cells and that this phenomenon is dependent on kinase-mediated activation of IRF3 in response to poly(I:C) treatment

(Figures 3D and 3E). We also show for the first time that blocking bat TBK1 and IKKϵ using an inhibitor reduces phosphorylation of the 396th serine residue in bat IRF3 (see Figures S1B and S1C) and subsequently dampens IRF3-S185-mediated antiviral protection against replicating VSV in bat cells (Figures 3D and 3E). It has been demonstrated that phosphorylation of S396 in human IRF3 alleviates autoinhibition and facilitates the phosphorylation of S385 and S386, thus amplifying the antiviral response (Panne et al., 2007). Similarly, phosphorylation of IRF3-S185 likely enhances phosphorylation of other serine residues in the serine-rich region that amplifies IRF3-mediated antiviral responses in bat and human cells. We also noted that treating bat cells with TBK1 and IKKϵ inhibitor did not restore VSV-GFP replication to levels observed in control cells (Figures 3D and 3E). It is possible that the kinase inhibitor is not as efficient in bat cells. Alternatively, we cannot rule out the presence of other kinases in bat cells that are capable of phosphorylating IRF3 in the absence of TBK1 and IKKϵ. Similarly, we observed that treating human cells with the kinase inhibitor did not restore virus replication to levels observed in control cells (Figure 3F). Since THF IRF3-KO cells were transfected with IRF3-S185 expressing plasmid prior to treatment with the inhibitor, the partial protection is likely due to plasmid-mediated upregulation of antiviral responses, which was observed in mock treated cells as well (Figure 3F). Further studies are required to identify the role of S185 in enhancing phosphorylation of additional serine residues in the serine-rich region of IRF3, along with any conformational changes that may be induced by the phosphorylation of S185 to facilitate additional phosphorylation events.

Loss of IRF3 has been linked to age-related cell senescence (Zhang et al., 2019), and a robust type I IFN response is associated with tumor regression and control (Hobeika et al., 1997). Bats display an exceptionally long lifespan (Foley et al., 2018; Huang et al., 2019; Wilkinson and Adams, 2019) and have evolved mechanisms that may mitigate tumor formation (Brook and Dobson, 2015). The role of IRF3 in aging and mitigation of tumorigenesis in bats is still speculative, but our data clearly demonstrate that IRF3 with S185 is a more potent inducer of antiviral responses in both bat and human cells. Future studies will elucidate on the possibility of leveraging knowledge from studies in bats to develop therapeutic strategies or enhanced therapeutic molecules for alternate mammalian species, such as humans.

LIMITATIONS OF THE STUDY

Owing to the lack of anti-phospho antibodies to S185 in IRF3, we were unable to verify the phosphorylation of S185. The lack of cell lines and reagents from additional bat species did not allow us to explore the role of S185 and other mutations in the serine-rich region of IRF3 in other species of bats. As IRF3 deleted cell lines from other bat species become available, it will be interesting to identify species-specific adaptations and the role of S185 in antiviral responses against emerging bat-borne RNA viruses, such as filoviruses, paramyxoviruses, and coronaviruses, including the recently emerged SARS-CoV-2. Another limitation of this study is the use of one non-bat cell line from humans. As more IRF3 knockout cell lines from additional mammalian species are generated, it will be interesting to observe the effect of S185 on IRF3-mediated antiviral responses.

METHODS

All methods can be found in the accompanying Transparent Methods supplemental file.

SUPPLEMENTAL INFORMATION

Supplemental Information can be found online at https://doi.org/10.1016/j.isci.2020.100958.

ACKNOWLEDGMENTS

A.B. is funded by M.G. DeGroote and Natural Sciences and Engineering Research Council of Canada (NSERC) fellowships (NSERC Grant ID: PDF - 532117–2019). A.Y. was supported by an NSERC summer scholarship. K.S.S. was supported by a DFG research fellowship from Germany. Work in L.-F.W.'s group is funded by the Singapore National Research Foundation grants (NRF2012NRF-CRP001-056). Studies in K.M.'s group were funded by an NSERC Discovery Grant.

AUTHOR CONTRIBUTIONS

Conceptualization, A.B., K.M., D.B. and B.G.; Methodology, A.B., X.Z., D.B., B.G. and K.M.; Investigation, A.B., X.Z., A.Y., D.B., B.G. and K.M.; Formal analysis, A.B., X.Z. and B.G.; Writing – original draft, A.B. and K.M.; Writing – reviewing & editing, A.B., D.B., B.G., A.T.I, L.-F.W. and K.M.; Visualization, A.B.; Funding

acquisition, K.M., A.B. and B.G.; Resources, A.B., K.S.S., A.T.I., B.G., L.-F.W. and K.M.; Supervision, A.B., D.B., B.G., and K.M.

DECLARATION OF INTERESTS

The authors declare no competing interests.

Received: January 8, 2020
Revised: January 13, 2020
Accepted: February 26, 2020
Published: March 27, 2020

REFERENCES

Ahn, M., Anderson, D.E., Zhang, Q., Tan, C.W., Lim, B.L., Luko, K., Wen, M., Chia, W.N., Mani, S., Wang, L.C., et al. (2019). Dampened NLRP3-mediated inflammation in bats and implications for a special viral reservoir host. Nat. Microbiol. *4*, 789–799.

Amman, B.R., Jones, M.E., Sealy, T.K., Uebelhoer, L.S., Schuh, A.J., Bird, B.H., Coleman-Mccray, J.D., Martin, B.E., Nichol, S.T., and Towner, J.S. (2015). Oral shedding of Marburg virus in experimentally infected Egyptian fruit bats (Rousettus aegyptiacus). J. Wildl. Dis. *51*, 113–124.

Anthony, S.J., Gilardi, K., Menachery, V.D., Goldstein, T., Ssebide, B., Mbabazi, R., Navarrete-Macias, I., Liang, E., Wells, H., Hicks, A., et al. (2017). Further evidence for bats as the evolutionary source of Middle East respiratory syndrome coronavirus. Mbio *8*, 1–13.

Ashley, C.L., Abendroth, A., Mcsharry, B.P., and Slobedman, B. (2019). Interferon-independent upregulation of interferon-stimulated genes during human cytomegalovirus infection is dependent on IRF3 expression. Viruses *11*, 1–13.

Banerjee, A., Baker, M.L., Kulcsar, K., Misra, V., Plowright, R., and Mossman, K. (2020). Novel insights into immune systems of bats. Front. Immunol. *11*, 1–15.

Banerjee, A., Falzarano, D., Rapin, N., Lew, J., and Misra, V. (2019). Interferon regulatory factor 3-mediated signaling limits Middle-East respiratory syndrome (MERS) coronavirus propagation in cells from an insectivorous bat. Viruses *11*, 1–21.

Banerjee, A., Rapin, N., Bollinger, T., and Misra, V. (2017). Lack of inflammatory gene expression in bats: a unique role for a transcription repressor. Sci. Rep. *7*, 2232.

Brook, C.E., and Dobson, A.P. (2015). Bats as 'special' reservoirs for emerging zoonotic pathogens. Trends Microbiol. *23*, 172–180.

Chen, X., Yang, X., Zheng, Y., Yang, Y., Xing, Y., and Chen, Z. (2014). SARS coronavirus papain-like protease inhibits the type I interferon signaling pathway through interaction with the STING-TRAF3-TBK1 complex. Protein Cell *5*, 369–381.

de La Cruz-Rivera, P.C., Kanchwala, M., Liang, H., Kumar, A., Wang, L.F., Xing, C., and Schoggins, J.W. (2018). The IFN response in bats displays distinctive IFN-stimulated gene expression kinetics with atypical RNASEL induction. J. Immunol. *200*, 209–217.

de Weerd, N.A., Samarajiwa, S.A., and Hertzog, P.J. (2007). Type I interferon receptors: biochemistry and biological functions. J. Biol. Chem. *282*, 20053–20057.

Ding, Z., Fang, L., Jing, H., Zeng, S., Wang, D., Liu, L., Zhang, H., Luo, R., Chen, H., and Xiao, S. (2014). Porcine epidemic diarrhea virus nucleocapsid protein antagonizes beta interferon production by sequestering the interaction between IRF3 and TBK1. J. Virol. *88*, 8936–8945.

Foley, N.M., Hughes, G.M., Huang, Z., Clarke, M., Jebb, D., Whelan, C.V., Petit, E.J., Touzalin, F., Farcy, O., Jones, G., et al. (2018). Growing old, yet staying young: the role of telomeres in bats' exceptional longevity. Sci. Adv. *4*, eaao0926.

Forbes, K.M., Webala, P.W., Jaaskelainen, A.J., Abdurahman, S., Ogola, J., Masika, M.M., Kivisto, I., Alburkat, H., Plyusnin, I., Levanov, L., et al. (2019). Bombali virus in mops condylurus bat, Kenya. Emerg. Infect. Dis. *25*, 955–957.

Ge, X.Y., Li, J.L., Yang, X.L., Chmura, A.A., Zhu, G., Epstein, J.H., Mazet, J.K., Hu, B., Zhang, W., Peng, C., et al. (2013). Isolation and characterization of a bat SARS-like coronavirus that uses the ACE2 receptor. Nature *503*, 535–538.

Hayman, D.T. (2016). Bats as viral reservoirs. Annu. Rev. Virol. *3*, 77–99.

Hobeika, A.C., Subramaniam, P.S., and Johnson, H.M. (1997). IFNalpha induces the expression of the cyclin-dependent kinase inhibitor p21 in human prostate cancer cells. Oncogene *14*, 1165–1170.

Hölzer, M., Schoen, A., Wulle, J., Müller, M.A., Drosten, C., Marz, M., and Weber, F. (2019). Virus- and interferon alpha-induced transcriptomes of cells from the microbat Myotis daubentonii. iScience *19*, 647–661.

Honda, K., Takaoka, A., and Taniguchi, T. (2006). Type I interferon [corrected] gene induction by the interferon regulatory factor family of transcription factors. Immunity *25*, 349–360.

Honda, K., and Taniguchi, T. (2006). IRFs: master regulators of signalling by Toll-like receptors and cytosolic pattern-recognition receptors. Nat. Rev. Immunol. *6*, 644–658.

Huang, Z., Whelan, C.V., Foley, N.M., Jebb, D., Touzalin, F., Petit, E.J., Puechmaille, S.J., and Teeling, E.C. (2019). Longitudinal comparative transcriptomics reveals unique mechanisms underlying extended healthspan in bats. Nat. Ecol. Evol. *3*, 1110–1120.

Johannsdottir, H.K., Mancini, R., Kartenbeck, J., Amato, L., and Helenius, A. (2009). Host cell factors and functions involved in vesicular stomatitis virus entry. J. Virol. *83*, 440–453.

Kawai, T., and Akira, S. (2006). Innate immune recognition of viral infection. Nat. Immunol. *7*, 131–137.

Leger, J., Kempf, M., Lee, G., and Brandt, R. (1997). Conversion of serine to aspartate imitates phosphorylation-induced changes in the structure and function of microtubule-associated protein tau. J. Biol. Chem. *272*, 8441–8446.

Lui, P.Y., Wong, L.Y., Fung, C.L., Siu, K.L., Yeung, M.L., Yuen, K.S., Chan, C.P., Woo, P.C., Yuen, K.Y., and Jin, D.Y. (2016). Middle East respiratory syndrome coronavirus M protein suppresses type I interferon expression through the inhibition of TBK1-dependent phosphorylation of IRF3. Emerg. Microbes Infect. *5*, e39.

Maxmen, A. (2017). Bats are global reservoir for deadly coronaviruses. Nature *546*, 340.

Munster, V.J., Adney, D.R., van Doremalen, N., Brown, V.R., Miazgowicz, K.L., Milne-Price, S., Bushmaker, T., Rosenke, R., Scott, D., Hawkinson, A., et al. (2016). Replication and shedding of MERS-CoV in Jamaican fruit bats (Artibeus jamaicensis). Sci. Rep. *6*, 21878.

Noyce, R.S., Taylor, K., Ciechonska, M., Collins, S.E., Duncan, R., and Mossman, K.L. (2011). Membrane perturbation elicits an IRF3-dependent, interferon-independent antiviral response. J. Virol. *85*, 10926–10931.

O'shea, T.J., Cryan, P.M., Cunningham, A.A., Fooks, A.R., Hayman, D.T., Luis, A.D., Peel, A.J., Plowright, R.K., and Wood, J.L. (2014). Bat flight and zoonotic viruses. Emerg. Infect. Dis. *20*, 741–745.

Panne, D., Mcwhirter, S.M., Maniatis, T., and Harrison, S.C. (2007). Interferon regulatory factor 3 is regulated by a dual phosphorylation-dependent switch. J. Biol. Chem. *282*, 22816–22822.

Pavlovich, S.S., Lovett, S.P., Koroleva, G., Guito, J.C., Arnold, C.E., Nagle, E.R., Kulcsar, K., Lee, A., Thibaud-Nissen, F., Hume, A.J., et al. (2018). The Egyptian rousette genome reveals unexpected features of bat antiviral immunity. Cell *173*, 1098–1110 e18.

Reilly, S.M., Chiang, S.H., Decker, S.J., Chang, L., Uhm, M., Larsen, M.J., Rubin, J.R., Mowers, J., White, N.M., Hochberg, I., et al. (2013). An inhibitor of the protein kinases TBK1 and IKK-varepsilon improves obesity-related metabolic dysfunctions in mice. Nat. Med. *19*, 313–321.

Sali, T.M., Pryke, K.M., Abraham, J., Liu, A., Archer, I., Broeckel, R., Staverosky, J.A., Smith, J.L., Al-Shammari, A., Amsler, L., et al. (2015). Characterization of a novel human-specific STING agonist that elicits antiviral activity against emerging alphaviruses. PLoS Pathog. *11*, e1005324.

Schountz, T., Baker, M.L., Butler, J., and Munster, V. (2017). Immunological control of viral infections in bats and the emergence of viruses highly pathogenic to humans. Front. Immunol. *8*, 1098.

Schuh, A.J., Amman, B.R., Jones, M.E., Sealy, T.K., Uebelhoer, L.S., Spengler, J.R., Martin, B.E., Coleman-Mccray, J.A., Nichol, S.T., and Towner, J.S. (2017). Modelling filovirus maintenance in nature by experimental transmission of Marburg virus between Egyptian rousette bats. Nat. Commun. *8*, 14446.

Simmons, N.B., Seymour, K.L., Habersetzer, J., and Gunnell, G.F. (2008). Primitive Early Eocene bat from Wyoming and the evolution of flight and echolocation. Nature *451*, 818–821.

Swanepoel, R., Smit, S.B., Rollin, P.E., Formenty, P., Leman, P.A., Kemp, A., Burt, F.J., Grobbelaar, A.A., Croft, J., Bausch, D.G., et al.; International Scientific and Technical Committee for Marburg Hemorrhagic Fever Control in the Democratic Republic of Congo (2007). Studies of reservoir hosts for Marburg virus. Emerg. Infect. Dis. *13*, 1847–1851.

Teeling, E.C., Springer, M.S., Madsen, O., Bates, P., O'brien S, J., and Murphy, W.J. (2005). A molecular phylogeny for bats illuminates biogeography and the fossil record. Science *307*, 580–584.

Uzé, G., Lutfalla, G., and Gresser, I. (1990). Genetic transfer of a functional human interferon α receptor into mouse cells: cloning and expression of its c-DNA. Cell *60*, 225–234.

Wilkinson, G.S., and Adams, D.M. (2019). Recurrent evolution of extreme longevity in bats. Biol. Lett. *15*, 20180860.

Wong, A., Li, X., Lau, S., and Woo, P. (2019). Global epidemiology of bat coronaviruses. Viruses *11*, 1–17.

Xie, J., Li, Y., Shen, X., Goh, G., Zhu, Y., Cui, J., Wang, L.F., Shi, Z.L., and Zhou, P. (2018). Dampened STING-dependent interferon activation in bats. Cell Host Microbe *23*, 297–301.e4.

Yang, X.L., Tan, C.W., Anderson, D.E., Jiang, R.D., Li, B., Zhang, W., Zhu, Y., Lim, X.F., Zhou, P., Liu, X.L., et al. (2019). Characterization of a filovirus (Mengla virus) from Rousettus bats in China. Nat. Microbiol. *4*, 390–395.

Yu, J., Zhou, X., Chang, M., Nakaya, M., Chang, J.H., Xiao, Y., Lindsey, J.W., Dorta-Estremera, S., CAO, W., ZAL, A., et al. (2015). Regulation of T-cell activation and migration by the kinase TBK1 during neuroinflammation. Nat. Commun. *6*, 6074.

Zhang, G., Cowled, C., Shi, Z., Huang, Z., Bishop-Lilly, K.A., Fang, X., Wynne, J.W., Xiong, Z., Baker, M.L., Zhao, W., et al. (2013). Comparative analysis of bat genomes provides insight into the evolution of flight and immunity. Science *339*, 456–460.

Zhang, X., Zhu, J., Chen, X., Jie-Qiong, Z., Li, X., Luo, L., Huang, H., Liu, W., Zhou, X., Yan, J., et al. (2019). Interferon regulatory factor 3 deficiency induces age-related alterations of the retina in young and old mice. Front. Cell Neurosci. *13*, 272.

Zhou, P., Cowled, C., Mansell, A., Monaghan, P., Green, D., Wu, L., Shi, Z., Wang, L.F., and Baker, M.L. (2014). IRF7 in the Australian black flying fox, *Pteropus alecto*: evidence for a unique expression pattern and functional conservation. PLoS One *9*, e103875.

Zhou, P., Tachedjian, M., Wynne, J.W., Boyd, V., Cui, J., Smith, I., Cowled, C., Ng, J.H., Mok, L., Michalski, W.P., et al. (2016). Contraction of the type I IFN locus and unusual constitutive expression of IFN-alpha in bats. Proc. Natl. Acad. Sci. U S A *113*, 2696–2701.

Zhou, P., yang, X.L., Wang, X.G., Hu, B., Zhang, L., Zhang, W., Si, H.R., Zhu, Y., Li, B., Huang, C.L., et al. (2020). A pneumonia outbreak associated with a new coronavirus of probable bat origin. Nature. https://www.nature.com/articles/s41586-020-2012-7.

iScience, Volume *23*

Supplemental Information

Positive Selection of a Serine Residue in Bat IRF3 Confers Enhanced Antiviral Protection

Arinjay Banerjee, Xi Zhang, Alyssa Yip, Katharina S. Schulz, Aaron T. Irving, Dawn Bowdish, Brian Golding, Lin-Fa Wang, and Karen Mossman

SUPPLEMENTAL ITEMS

FIGURE

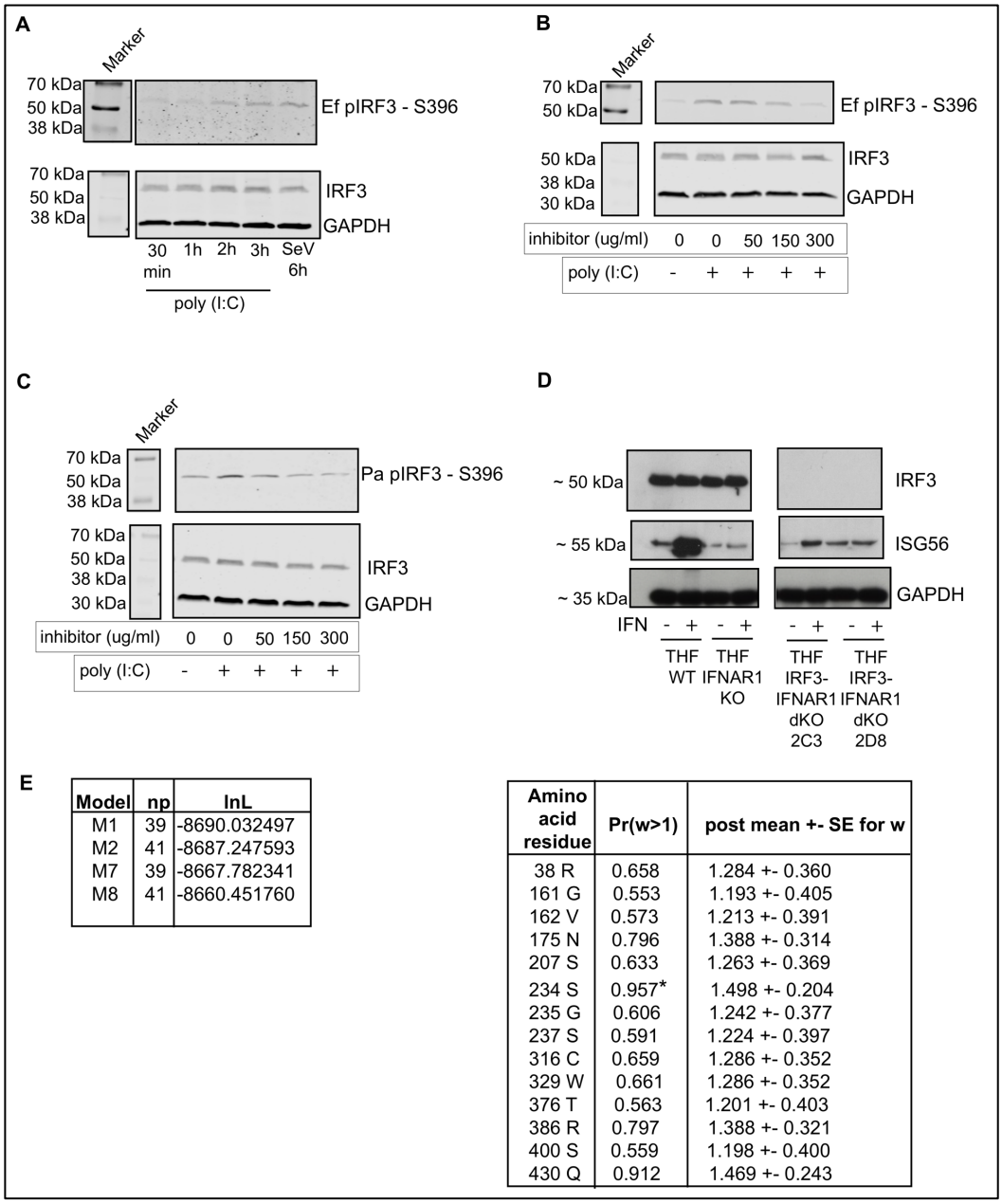

E

Model	np	lnL
M1	39	-8690.032497
M2	41	-8687.247593
M7	39	-8667.782341
M8	41	-8660.451760

Amino acid residue	Pr(w>1)	post mean +- SE for w
38 R	0.658	1.284 +- 0.360
161 G	0.553	1.193 +- 0.405
162 V	0.573	1.213 +- 0.391
175 N	0.796	1.388 +- 0.314
207 S	0.633	1.263 +- 0.369
234 S	0.957*	1.498 +- 0.204
235 G	0.606	1.242 +- 0.377
237 S	0.591	1.224 +- 0.397
316 C	0.659	1.286 +- 0.352
329 W	0.661	1.286 +- 0.352
376 T	0.563	1.201 +- 0.403
386 R	0.797	1.388 +- 0.321
400 S	0.559	1.198 +- 0.400
430 Q	0.912	1.469 +- 0.243

Figure S1. Phosphorylation of IRF3, efficacy of TBK1 and IKKε inhibitor in bat cells, details on computational analysis and validation of IRF3 KO THF cells, Related to Figures 1 and 3, and STAR METHODS. (A) Determination of IRF3-S396 phosphorylation using a cross-reactive human pIRF3-S396 antibody. Efk3B cells were treated with 100 ng of poly(I:C) and cell lysates were harvested at multiple time points. Efk3B cells were also infected with Sendai virus for 6 h and cell lysates were harvested for immunoblots. Immunoblots for the 396th phospho-serine residue in IRF3 (pIRF3-S396), IRF3 and GAPDH are shown. Lanes 2-5 were removed from this blot. The deletion between the ladder and lanes 6-10 is indicated by a space.

(B) Efk3B cells were mock treated or treated with increasing concentrations of TBK1 and IKKε inhibitor (Amlexanox), and mock stimulated or stimulated with 100 ng of poly(I:C). Cell lysates were harvested for immunoblots. Immunoblots for pIRF3-S396, IRF3 and GAPDH are shown. Lanes 2-4 were removed from this blot. The deletion between the ladder and lanes 5-9 is indicated by a space.

(C) PakiT03 cells were mock treated or treated with increasing concentrations of TBK1 and IKKε inhibitor (Amlexanox), and mock stimulated or stimulated with 100 ng of poly(I:C). Cell lysates were harvested for immunoblots. Immunoblots for pIRF3-S396, IRF3 and GAPDH are shown. Lanes 2-4 were removed from this blot. The deletion between the ladder and lanes 5-9 is indicated by a space.

(D) Related to STAR Methods. Validation of *IRF3* and *IFNAR1* knockout in THF-IRF3-IFNAR1 double knockout (dKO) cells. IRF3, ISG56 and GAPDH protein expression were detected by immunoblots in mock-treated cells or cells treated with human leukocyte interferon for 1 hour. THF WT and THF-IFNAR1 KO cells were used as positive and negative controls, respectively for IFN-induced ISG56 expression. Different portions of the gels are represented here, separated by spaces. The blots were developed using chemiluminescent technology (see methods). Approximate sizes of the proteins are indicated.

(E) Related to Figure 1. Using the Python ETE3 package, the aligned sequences were tested for positive selection using PAML models. The results for IRF3 are shown. Model M1 was tested against M2. These models differ, with the later having an extra parameter with omega (w) greater than zero (indicating positive selection). The significantly increased likelihood indicates that a model with positive selection fits better (left panel). Model M7 was tested against M8. These models have categories that follow a beta distribution, while M8 allows for positive selection. The significantly increased likelihood indicates positive selection fits better. Since the likelihood ratios were significant (left panel), posterior probabilities were used to identify sites under positive selection. The differences, M7/M8, via Bayes Empirical Bayes (BEB) analysis (Yang et al., 2005) identified positively selected sites that are shown in the right panel. The sites are numbered according to *Bos taurus* IRF3 sequence. The Serine (S) residue at position 234 (234 S) corresponds to site 185 in Figure 1 and has an omega value significantly >1.

Ef, *Eptesicus fuscus*; Pa, *Pteropus alecto*; pIRF3, phospho-IRF3; WT, wildtype; IFNAR, interferon α/β receptor; dKO, double knockout; IRF3, interferon regulatory factor 3, GAPDH, Glyceraldehyde 3-phosphate dehydrogenase; ISG56, Interferon-stimulated gene 56.

TABLES

Table S1. Primer and guide RNA sequences used in this study, Related to STAR Methods.

Cloning and site-directed mutagenesis	**Forward primer**	**Reverse primer**
Clone human IRF3	GCCGCTAGCGCCACCATGGGAACCCCAAAG	GCCCTCGAGTCAGGTCTCCCCAGG
Clone *E. fuscus* IRF3	GCCGCTAGCGCCACCATGGGATCCCAG	GCCGAATTCCTAGAAATCCATG
Clone *P. alecto* IRF3	GCCGCTAGCGCCACCATGGCTACCCCAAAGC	GCCCTCGAGCTAGAAATCCATGTCC
Site-directed mutagenesis - human IRF3-S185	ACTCCCTTCCCAAACAGTGGGCCCTCTGAGAAC	GTTCTCAGAGGGCCCACTGTTTGGGAAGGGAGT
Site-directed mutagenesis - *E. fuscus* IRF3-L185	GCTCCCTACCCAAACCTAGGACCCCCTGAAAAC	GTTTTCAGGGGGTCCTAGGTTTGGGTAGGGAGC
Site-directed mutagenesis - *P. alecto* IRF3-L185	GCTCCCTGCCCAAACCTAGAACCCCCTGAAAAC	GTTTTCAGGGGGTTCTAGGTTTGGGCAGGGAGC
Site-directed mutagenesis - human IRF3-D185	ACTCCCTTCCCAAACGACGGGCCCTCTGAGAAC	GTTCTCAGAGGGCCCGTCGTTTGGGAAGGGAGT
Site-directed mutagenesis - *E.*	GCTCCCTACCCAAACGACGGACCCCCTGAAAAC	GTTTTCAGGGGGTCCGTCGTTTGGGTAGGGAGC

fuscus IRF3-D185		
Site-directed mutagenesis - *P. alecto* IRF3-D185	GCTCCCTGCCCAAACGACGAACCCCCTGAAAAC	GTTTTCAGGGGGTTCGTCGTTTGGGCAGGGAGC
Generating CRISPR KO cells	**Guide RNA sequence**	
THF IRF3-IFNAR1 dKO cells	IFNAR1 gRNA: AAACACTTCTTCATGGTATG	
PakiT03 - 4G (IRF3 KO cells)	Pa-IRF3-gRNA1-F1: CACCGTTGGAAGCACGGCTTGCGGC	Pa-IRF3-gRNA1-R1: AAACGCCGCAAGCCGTGCTTCCAAC
PakiT03-IFNAR2-IRF3-G6 dKO cells	Pa-IRF3-gRNA1-F1: CACCGTTGGAAGCACGGCTTGCGGC	Pa-IRF3-gRNA1-R1: AAACGCCGCAAGCCGTGCTTCCAAC
Validating CRISPR edited KO cells	**Primers to verify deletion/mutation in guide RNA binding site**	
	Forward primer	**Reverse primer**
PakiT03 - 4G (IRF3 KO cells)	CACCGTTGGAAGCACGGCTTGCGGC	CACCGTTGGAAGCACGGCTTGCGGC
PakiT03-IFNAR2-IRF3-G6 (IFNAR2 and IRF3 dKO cells)	CACCGTTGGAAGCACGGCTTGCGGC	CACCGTTGGAAGCACGGCTTGCGGC
THF IRF3-IFNAR1 dKO	AACAGGAGCGATGAGTCTGTC	TGCGAAATGGTGTAAATGAGTCA

Sequencing CRISPR edited *P. alecto* and THF cells	**Guide RNA binding site sequence in CRISPR edited clonal cell population**	
PakiT03-4G (IRF3 KO)	IRF3-4G: -23 bp deletion in IRF3 coding sequences, homozygous CGCAGGTTGGACCATGGCTACCCCAAA GCCGAGGATCCTGCCCTGGCTAGTGTC GCAGCTGGACAGTGGGCAGCTGGAGGG CGTGGCATGGCTGAACGAGAGCCGCAC GCGCTTTCGCATCCCTTGGAAGCACGGC TTGCGGCAGGATGCCCAGCAGGAGGAC TTCGGCATCTTCCAGGTGCGCAGGAGC CAAGACTGGGCAAACACGGGGCGGGGC GGACTCCGAGGGCACTG	
PakiT03-IFNAR2-IRF3-G6 (IFNAR2 IRF3 dKO)	IRF3-/- IFNAR-/-: +1bp insertion in IRF3 coding sequence, homozygous CAGCTGGAGGGCGTGGCATGGCTGAAC GAGAGCCGCACGCGCTTTCGCATCCCTT GGAAGCACGGCTTGCCGGCAGGATGCC CAGCAGGAGGACTTCGGCATCTTCCAG GTGCGCAGGAG	
THF IRF3-IFNAR1 dKO	+2 bp insertion in IFNAR1 coding sequence TGACTCATTTACACCATTTCGCAAAGCT CAGATTGTGTCCTCCAGCAGTGAATGTT TAAATTTAAACGAATCGGAAGATCGGT AATTATTTGAT	

Table S2. NCBI accession numbers of IRF3 amino acid sequences used in phylogenetic and evolutionary analyses, Related to Figure 1.

Mammal	**IRF3 sequence accession number**
Pongo abelii	XP_009231174.2
Homo sapiens	XP_016882256.1
Equus caballus	XP_014585307.1
Desmodus rotundus	XP_024422099.1
Miniopterus natalensis	XP_016061535.1
Eptesicus fuscus	XP_008152570.1
Myotis davidii	XP_015420914.1
Myotis lucifugus	XP_014305320.1
Myotis brandtii	XP_005879595.1
Hipposideros armiger	XP_019513839.1
Rhinolophus sinicus	XP_019597087.1
Rousettus aegyptiacus	XP_015977865.1
Pteropus vampyrus	XP_011372830.1
Pteropus alecto	XP_006905084.1
Sus scrofa	NP_998935.1
Bos taurus	XP_024833997.1
Mus musculus	NP_058545.1
Cricetulus griseus	XP_027276506.1
Macaca fascicularis	XP_005589990.1
Macaca mulatta	NP_001129269.1

TRANSPARENT METHODS

Key Resources Table

REAGENT or RESOURCE	SOURCE	IDENTIFIER
Antibodies		
Rabbit anti-IRF3	Abcam	Cat#ab68481; RRID: AB_11155653
Rabbit anti-pIRF3-S396	Cell Signaling technology	Cat# 4947S; RRID: AB_823547
Mouse anti-GAPDH	EMD Milipore	Ca#AB2302; RRID: AB_10615768
Donkey anti-Rabbit 800	LI-COR	Cat#926-32213; RRID: 621848
Goat anti-mouse 680	LI-COR	Cat#925-68070; RRID: AB_2651128
Rabbit anti-IRF3 (FL-425)	Santa Cruz	Cat#sc-9082
Rabbit anti-ISG56	Laboratory of Dr. Ganes Sen	(Guo et al., 2000)
Mouse anti-GAPDH	Santa Cruz	Cat#sc-47724; RRID: AB_627678
Goat anti-mouse (peroxidase conjugated)	SIGMA	Cat#A8786; RRID: AB_258413
Goat anti-rabbit (peroxidase conjugated)	SIGMA	A0545; RRID: AB_257896
Virus strain		
Vesicular stomatitis virus - GFP (VSV-GFP)	Laboratory of Brian Lichty	(Leveille et al., 2011)
Sendai virus	Laboratory of Karen Mossman	(Noyce et al., 2006)
Chemicals		
Poly(I:C) (HMW)	InvivoGen	Cat#tlrl-pic
Lipofectamine 3000	Invitrogen	Cat#L3000015
Interferon from human leukocytes	Sigma-Aldrich	Cat#I4784
Amlexanox (TBK1 and IKKε inhibitor)	InvivoGen	Cat#inh-amx
Critical Commercial Assays		
QuikChange II site-directed mutageneisis	Agilent	Cat#200524-5

Q5 High-fidelity DNA polymerase	New England Biolabs	Cat#M0491S
Experimental models: cell lines		
cr3-8	Laboratory of Vikram Misra	(Banerjee et al., 2019)
THF-IRF3 KO	Laboratory of Victor DeFilippis	(Sali et al., 2015)
PakiT03 - 4G (IRF3 KO)	This study	NA
THF-IRF3-IFNAR1 dKO (double knockout)	This study	NA
PaKiT03-IFNAR2-IRF3-G6 dKO	This study	NA
Efk3B	Laboratory of Vikram Misra	(Banerjee et al., 2016) RRID: CVCL_GZ34
PakiT03	Laboratory of Lin-fa Wang	(Zhang et al., 2017) RRID: CVCL_DR89
PakiT03-IFNAR2-4A	Laboratory of Lin-fa Wang	(Zhang et al., 2017)
THF	Laboratory of Victor DeFilippis	(DeFilippis et al., 2010)
HEK293T	Laboratory of Brian D. Lichty	(Wang et al., 2016)
THF-IFNAR1 KO	Laboratory of Victor DeFilippis	(Pryke et al., 2017)
Oligonucleotides		
Primers for IRF3 cloning and mutagenesis, see Table S1	This study	NA
Recombinant DNA		
pcDNA3.1	ThermoFisher Scientific	Cat#V79020
pcDNA3.1 hu IRF3-WT	This study	NA

pcDNA3.1 hu IRF3-L185S	This study	NA
pcDNA3.1 Ef IRF3-WT	This study	NA
pcDNA3.1 Ef IRF3-S185L	This study	NA
pcDNA3.1 Pa IRF3-WT	This study	NA
pcDNA3.1 Pa IRF3-S185L	This study	NA
pcDNA3.1 hu IRF3-L185D	This study	NA
pcDNA3.1 Ef IRF3-S185D	This study	NA
pcDNA3.1 Pa IRF3-S185D	This study	NA
psPAX2	Addgene	Cat#12260
pMD2.G	Addgene	Cat#12259
plentiCRISPR hygro IFNAR	Laboratory of Victor DeFilippis	(Pryke et al., 2017)
Softwares and algorithms		
Prism software	GraphPad	https://www.graphpad.com
Image studio	LI-COR	https://www.licor.com/bio/image-studio/
Guide RNA design resources	Broad Institute	http://tools.genome-engineering.org

CONTACT FOR REAGENT AND RESOURCE SHARING

Dr. Karen Mossman (mossk@mcmaster.ca) and Dr. Lin-Fa Wang (linfa.wang@duke-nus.edu.sg).

COMPUTATIONAL ANALYSIS

The longest IRF3 isoform for each of eleven bat species was selected from the NCBI nucleotide database . A group of diverse species of mammals were selected to serve as outgroups. These included primates (*Homo sapiens*, *Macaca mulatta*, *Macaca fascicularis* and *Pongo abelli*), rodents (*Mus musculus*, and *Cricetulus griseus*), *Equus ferus, Bos taurus* and *Sus scrofa*. The alignments were carried out using MAFFT (version 7 with the G-INS-i (globalpair –maxiterate 1000) option) (Katoh et al., 2002). The alignment was manually checked using NCBI's multiple sequence alignment (MSA) viewer and checked to ensure that all codons were correctly aligned. RAxML HPC (version 8.2) was used to generate phylogenetic trees using amino acid sequences (Stamatakis, 2014). Phylogenetic trees were generated using the WAG matrix (GAMMA model). For each tree, 1000 bootstraps were generated. A majority consensus (>50%) tree was then calculated from the bootstrap trees. PAML CodeML v4.5 was automated by ETE3 package under Python 2.7 environment (Yang, 2007, Yang, 1997). Branch lengths were calculated by

CodeML. Site selection models (M1a, M2a, M7, M8) and branch-site model as specified by CodeML were tested. For the branch-site model, each branch, which consists of a single species was tested for positive selection. A likelihood ratio test was used to test the difference between the alternate and null hypothesis. M1 is the nearly neutral model, and was the null hypothesis that was tested against M2, which incorporates positive selection. Model M7 incorporates a beta distributed selection values while M8 adds a class of sites with positive selection. Model M8 was tested against the null hypothesis M7. Since the likelihood ratios were significant (see supplementary figure S1E; left panel), posterior probabilities were used to identify sites under positive selection. The differences, M7/M8, via Bayes Empirical Bayes (BEB) analysis (Yang et al., 2005) identified positively selected residues (see supplementary figure S1E; right panel).

EXPERIMENTAL MODEL

Viruses and Cell lines

THF, THF-IRF3 knockout (KO), THF-IFNAR1 KO, THF-IRF3-IFNAR1 double-KO (dKO) human fibroblast cells and HEK 293T cells were maintained in Dulbecco's modified Eagle medium (DMEM; Sigma) supplemented with L-Glutamine (Sigma), 10% fetal bovine serum (FBS; Sigma) and penicillin/streptomycin (ThermoFisher Scientific). Efk3B (wildtype cells) and cr3-8 (*E. fuscus* IRF3KO kidney) cells were maintained in DMEM supplemented with GlutaMax (Gibco), 10% FBS and penicillin/streptomycin. PakiT03, PakiT03-4G (IRF3 KO), PakiT03-IFNAR2-4A and PakiT03-IFNAR2-IRF3-G6 dKO cells (*P. alecto* kidney cells) were maintained in DMEM supplemented with GlutaMax (Gibco), 10% FBS and penicillin/streptomycin. All cells were incubated at 37°C in humidified, 5% CO_2 incubators. Cell lines were periodically tested for mycoplasma contamination. Stocks of genetically engineered vesicular stomatitis virus (VSV-GFP) carrying a GFP expression cassette (Noyce et al., 2011) were stored at -80°C. Virus stocks were thawed once and used for an experiment. A fresh vial was used for each experiment to avoid repeated freeze-thaws.

Generation and validation of CRISPR knockout cells

THF-IRF3-IFNAR1 double-KO (dKO) cells were generated by knocking out *IFNAR1* in previously published THF-IRF3 KO cells (DeFilippis et al., 2006). Lentivirus transduction was used to express Cas9 and guide RNA (gRNA) targeting *IFNAR1* in THF-IRF3 KO cells. Briefly, previously published transfer vector (plentiCRISPR hygro IFNAR) containing *IFNAR1* guide RNA (gRNA) and Cas9 (Pryke et al., 2017) (a gift from Victor DeFilippis' laboratory), and packaging plasmids psPAX2 (Addgene) and pMD2.G (Addgene) were transfected into HEK 293T cells using Lipofectamine 3000 (Invitrogen) (see Table S1 for gRNA sequence). 6 h post transfection, the transfection mixture was replaced with complete media containing 1% BSA. 60 h post transfection, the supernatant was harvested and virus was concentrated by ultracentrifugation. THF-IRF3 KO cells were infected with the lentivirus in complete media containing 0.1% polybrene. The following day, cells were passaged and seeded in 10 cm dishes in complete media containing hygromycin. 10 days later, single cell clones were selected and cultured over time. To characterize THF-IRF3-IFNAR1 dKO cells, we were unable to validate the knockout of IFNAR1 by immunoblots since commercially available antibodies did not cross-react with human IFNAR1. To overcome this limitation, we performed immunoblots to demonstrate the loss of IFNAR1-mediated downstream IFNα signalling and ISG56 expression in these cells (see supplementary figure S1D). Briefly, THF-WT, THF-IFNAR1 KO and THF-IRF3-IFNAR1 dKO cells were treated with interferon from human leukocytes (Sigma) for 1 h and cell lysates were harvested for immunoblots. 25 μg of total protein per sample was analyzed

by immunoblot for ISG56 and IRF3 protein expression. THF IRF3-IFNAR1 dKO clone 2D8 was used for subsequent studies.

For PakiT03-4G (IRF3KO) and PakiT03-IFNAR2-IRF3-G6 dKO cells, guide RNA design, vector construction, transfection, single cell screening and validation were done as previously described (Zhang et al., 2017). Parental *P. alecto* kidney cells (PakiT03) were used to generate *IRF3* knockout cells (PakiT03-4G). Similarly, previously published *P. alecto IFNAR2* knockout (PakiT03-IFNAR2-4A) cells (Zhang et al., 2017) were used to generate *IFNAR2* and *IRF3* double knockout cells (PakiT03-IFNAR2-IRF3-G6 dKO). To generate guide RNA targeting *IRF3*, exon sequence of *IRF3* was submitted to an online software (http://tools.genome-engineering.org) to obtain potential gRNA targets (see Table S1 for gRNA sequences). The top hits were further subjected to BLAST (NCBI) analysis against *P.alecto* genome to exclude off-target effects. Two gRNA sequences with high score and specificity were chosen for plasmid construction. The pSpCas9 (BB)-2A-GFP plasmid was used as a vector as previously published (Ran et al., 2013). *P. alecto* immortalized kidney (PaKiT03) cell lines (Crameri et al., 2009) were seeded in 6-well plates at a concentration of 8×10^5 cells/well and transfected with 1.5 µg of plasmid using Lipofectamine 3000 (Life Technologies, Carlsbad, CA, USA) as per manufacturer's recommendation. Two days after transfection, cells were sorted using FACSAria III (BD Biosciences). GFP-positive clones were collected and seeded in 96-well plates at a concentration of approximately 2 cells/well. One week later, single colonies of cells were selected for further validation using fluorescent capillary gel electrophoresis. Briefly, genomic DNA from clonal cell populations was extracted using QuickExtract solution (Epicentre) and genetic modifications were verified by PCR, followed by sequencing as previously described (Zhang et al., 2017) (see Table S1). In addition, THF-IRF3-KO and THF-IRF3-IFNAR1 dKO cells were validated using functional assays as part of this study (Figures 2D and 4A). Similarly, PakiT03-4G and PakiT03-IFNAR2-IRF3-G6 dKO cells were also validated by immunoblots and functional assays as part of this study (Figures 2C, 4C and 4D).

METHOD DETAILS

Plasmid construction

RNA was extracted from wildtype THF (human fibroblast), Efk3B (*E. fuscus* kidney cells) and PakiT03 (*P. alecto* kidney cells) cells using the RNeasy RNA extraction kit (Qiagen). cDNA was prepared from 500 ng of RNA using iScript gDNA clear cDNA synthesis kit (Bio-Rad). IRF3 coding sequences were amplified using a high-fidelity Q5 DNA polymerase (New England BioLabs) and species-specific primers with restriction sites (see Table S1 for primers). IRF3 amplicons were cloned into pcDNA3.1 (ThermoFisher Scientific) expression plasmid using restriction digestion (New England Biolabs), followed by ligation with T4 DNA ligase (Invitrogen). Restriction enzymes NheI and EcoRI (New England Biolabs) were used to digest *E. fuscus* IRF3 amplicon. NheI and XhoI (New England Biolabs) were used to digest human and *P. alecto* IRF3 amplicons. All plasmid constructs were confirmed by sequencing (Mobix).

Site-directed mutagenesis

Site-directed mutagenesis was performed using the QuikChange II site-directed mutagenesis kit (Agilent). Wang and Malcolm's modification of the manufacturer's protocol was used for this assay (Wang W, 1999). See Table S1 for primer information. Mutations were confirmed by sequencing (Mobix).

Transfection
IRF3 expression plasmids and poly(I:C) were transfected using Lipofectamine 3000 reagent as per manufacturer's recommendation (Invitrogen). Varying concentrations of IRF3 expression plasmids or 200 ng of empty (pcDNA 3.1) control plasmid were transfected for 24 hrs. After 24 hrs, media on the cells was replaced with fresh growth media and cells were either mock transfected or transfected with poly(I:C) for 6 hrs. 10 ng poly(I:C) was used for *E. fuscus* (cr3-8) and human (THF and all CRISPR/clonal derivatives) cell lines. After optimizing poly(I:C)-mediated antiviral responses in *P. alecto* cells (PakiT03 and all CRISPR/clonal derivatives), an optimal concentration of 100 ng was used for all studies in cells from this bat.

Virus infection and quantification
2 x 10^5 cells/well were seeded in 12-well plates and incubated overnight at 37°C with 5% CO_2. Following IRF3 or empty plasmid transfection for 24 hrs and subsequent 6 hrs of poly(I:C) or mock stimulation, cells were either mock infected or infected with VSV-GFP in serum-free media. Human and *E. fuscus* cells were infected with 5.5 x 10^4 $TCID_{50}$/ml of VSV-GFP. *P. alecto* cells were infected with 2.75 x 10^3 $TCID_{50}$/ml of VSV-GFP. For IRF3-S396 phosphorylation assay in *E. fuscus cells,* Efk3B cells were infected with 80 HA units of Sendai virus. Infected cells were incubated at 37°C for 1 hr with gentle rocking every 15 minutes. After 1 hr, virus inoculum was aspirated and Minimum Essential Medium (MEM) with Earle's salts (Sigma) containing 2% FBS and 1% carboxymethyl cellulose (CMC; Sigma) was added on the cells. The plates were incubated for 19 hrs (VSV-GFP) at 37°C and green fluorescent protein (GFP) levels were measured using a typhoon scanner (Amersham). Sendai virus infected cells were incubated for 6 hrs and cell lysates were processed for immunoblots.

Immunoblots
Cells were seeded at a concentration of 2 × 10^5 cells/well in 12-well plates and transfected with varying concentrations of IRF3 expression plasmids. Cells were harvested 24 hrs after transfection. Samples were denatured in a reducing sample buffer and analyzed on a reducing gel. Proteins were blotted from the gel onto polyvinylidene difluoride (PVDF) membranes (Immobilon, Milipore) and detected using primary and secondary antibodies. Primary antibodies used were: 1:1000 mouse anti-GAPDH (EMD Milipore; Catalogue number: AB2302; RRID: AB_10615768), 1:1000 rabbit anti-IRF3 (Abcam; Catalogue number: ab68481; RRID: AB_11155653) and 1:1000 rabbit anti-pIRF3-S396 (Cell Signaling technology; Catalogue number: 4947S; RRID: ab_823547). Secondary antibodies used were: 1:5000 donkey anti-rabbit 800 (LI-COR Biosciences; Catalogue number: 926-32213; RRID: 621848) and 1:5000 goat anti-mouse 680 (LI-COR Biosciences; Catalogue number: 925-68070; RRID: AB_2651128). Blots were observed and imaged using Image Studio (LI-COR Biosciences) on the Odyssey CLx imaging system (LI-COR Biosciences). For the detection of ISG56, GAPDH and IRF3 in THF and CRISPR/Cas9 modified THF cells (Figure S1D), enhanced luminol-based chemiluminescence was used as previously described (Noyce et al., 2006). Primary antibodies used were: 1:1000 rabbit anti-IRF3 (Santa Cruz; Catalogue number: sc-9082; RRID: AB_2264929), mouse anti-GAPDH (Santa Cruz; Catalogue number: sc-47724; RRID: AB_627678) and rabbit anti-ISG56 (gift from Dr. Ganes Sen). Peroxidase conjugated goat anti-rabbit (Sigma; Catalogue number: A0545; RRID: AB_257896) and goat anti-mouse (Sigma; Catalogue number: A8786; RRID: AB_258413) secondary antibodies were used for the chemiluminescent immunoblots. Films were scanned on a typhoon scanner (Amersham).

TBK1 and IKKε inhibitor treatment

1.5×10^5 cells/well were seeded in 12-well plates and incubated at 37ºC and 5% CO_2. 24 hrs after seeding cells, 100 ng of IRF3-S185 expression plasmids were transfected into cells. After 24 hrs, media was changed and cells were wither mock treated with DMSO or treated with various concentrations of the inhibitor (Amlexanox, InvivoGen) for 1 hr at 37ºC. After 1 hr, cells were mock treated or transfected with poly(I:C). 3-6 hrs after poly(I:C) transfection, cells were harvested for immunoblots or infected with VSV-GFP.

QUANTIFICATION AND STATISTICAL ANALYSIS

Immunoblot quantification

Immunoblot bands were quantified using Image Studio (LI-COR Biosciences).

Statistical Analysis

Data analysis were performed using SPSS statistics package version 21. All data are shown as Mean ± SD. Statistical analysis was performed using Student's t test with two-tailed, 95% confidence. P values less than 0.05 were considered statistically significant (* $p < 0.05$, ** $p < 0.01$ and *** $p < 0.001$). 'n' represents number of experimental replicates that were carried out and are specified in the figure legends.

REFERENCES

BANERJEE, A., FALZARANO, D., RAPIN, N., LEW, J. & MISRA, V. 2019. Interferon Regulatory Factor 3-Mediated Signaling Limits Middle-East Respiratory Syndrome (MERS) Coronavirus Propagation in Cells from an Insectivorous Bat. *Viruses,* 11.

BANERJEE, A., RAPIN, N., MILLER, M., GRIEBEL, P., ZHOU, Y., MUNSTER, V. & MISRA, V. 2016. Generation and Characterization of Eptesicus fuscus (Big brown bat) kidney cell lines immortalized using the Myotis polyomavirus large T-antigen. *J Virol Methods,* 237**,** 166-173.

CRAMERI, G., TODD, S., GRIMLEY, S., MCEACHERN, J. A., MARSH, G. A., SMITH, C., TACHEDJIAN, M., DE JONG, C., VIRTUE, E. R., YU, M., BULACH, D., LIU, J. P., MICHALSKI, W. P., MIDDLETON, D., FIELD, H. E. & WANG, L. F. 2009. Establishment, immortalisation and characterisation of pteropid bat cell lines. *PLoS One,* 4**,** e8266.

DEFILIPPIS, V. R., ROBINSON, B., KECK, T. M., HANSEN, S. G., NELSON, J. A. & FRUH, K. J. 2006. Interferon regulatory factor 3 is necessary for induction of antiviral genes during human cytomegalovirus infection. *J Virol,* 80**,** 1032-7.

DEFILIPPIS, V. R., SALI, T., ALVARADO, D., WHITE, L., BRESNAHAN, W. & FRUH, K. J. 2010. Activation of the interferon response by human cytomegalovirus occurs via cytoplasmic double-stranded DNA but not glycoprotein B. *J Virol,* 84**,** 8913-25.

GUO, J., PETERS, K. L. & SEN, G. C. 2000. Induction of the human protein P56 by interferon, double-stranded RNA, or virus infection. *Virology,* 267**,** 209-19.

KATOH, K., MISAWA, K., KUMA, K. & MIYATA, T. 2002. MAFFT: a novel method for rapid multiple sequence alignment based on fast Fourier transform. *Nucleic Acids Res,* 30**,** 3059-66.

LEVEILLE, S., GOULET, M. L., LICHTY, B. D. & HISCOTT, J. 2011. Vesicular stomatitis virus oncolytic treatment interferes with tumor-associated dendritic cell functions and abrogates tumor antigen presentation. *J Virol,* 85**,** 12160-9.

NOYCE, R. S., COLLINS, S. E. & MOSSMAN, K. L. 2006. Identification of a novel pathway essential for the immediate-early, interferon-independent antiviral response to enveloped virions. *J Virol,* 80**,** 226-35.

NOYCE, R. S., TAYLOR, K., CIECHONSKA, M., COLLINS, S. E., DUNCAN, R. & MOSSMAN, K. L. 2011. Membrane perturbation elicits an IRF3-dependent, interferon-independent antiviral response. *J Virol,* 85**,** 10926-31.

PRYKE, K. M., ABRAHAM, J., SALI, T. M., GALL, B. J., ARCHER, I., LIU, A., BAMBINA, S., BAIRD, J., GOUGH, M., CHAKHTOURA, M., HADDAD, E. K., KIRBY, I. T., NILSEN, A., STREBLOW, D. N., HIRSCH, A. J., SMITH, J. L. & DEFILIPPIS, V. R. 2017. A Novel Agonist of the TRIF Pathway Induces a Cellular State Refractory to Replication of Zika, Chikungunya, and Dengue Viruses. *MBio,* 8.

RAN, F. A., HSU, P. D., WRIGHT, J., AGARWALA, V., SCOTT, D. A. & ZHANG, F. 2013. Genome engineering using the CRISPR-Cas9 system. *Nat Protoc,* 8**,** 2281-2308.

SALI, T. M., PRYKE, K. M., ABRAHAM, J., LIU, A., ARCHER, I., BROECKEL, R., STAVEROSKY, J. A., SMITH, J. L., AL-SHAMMARI, A., AMSLER, L., SHERIDAN, K., NILSEN, A., STREBLOW, D. N. & DEFILIPPIS, V. R. 2015. Characterization of a Novel Human-Specific STING Agonist that Elicits Antiviral Activity Against Emerging Alphaviruses. *PLoS Pathog,* 11**,** e1005324.

STAMATAKIS, A. 2014. RAxML version 8: a tool for phylogenetic analysis and post-analysis of large phylogenies. *Bioinformatics,* 30**,** 1312-3.

WANG, F., ALAIN, T., SZRETTER, K. J., STEPHENSON, K., POL, J. G., ATHERTON, M. J., HOANG, H. D., FONSECA, B. D., ZAKARIA, C., CHEN, L., RANGWALA, Z., HESCH, A., CHAN, E. S. Y., TUINMAN, C., SUTHAR, M. S., JIANG, Z., ASHKAR, A. A., THOMAS, G., KOZMA, S. C., GALE, M., JR., FITZGERALD, K. A., DIAMOND, M. S., MOSSMAN, K., SONENBERG, N., WAN, Y. & LICHTY, B. D. 2016. S6K-STING interaction regulates cytosolic DNA-mediated activation of the transcription factor IRF3. *Nat Immunol,* 17**,** 514-522.

WANG W, M. B. 1999. Two-stage PCR protocol allowing introduction of multiple mutations, deletions and insertions using QuikChange Site-Directed Mutagenesis. *Biotechniques,* 26**,** 680-682.

YANG, Z. 1997. PAML: a program package for phylogenetic analysis by maximum likelihood. *Bioinformatics,* 13**,** 555-556.

YANG, Z. 2007. PAML 4: phylogenetic analysis by maximum likelihood. *Mol Biol Evol,* 24**,** 1586-91.

YANG, Z., WONG, W. S. & NIELSEN, R. 2005. Bayes empirical bayes inference of amino acid sites under positive selection. *Mol Biol Evol,* 22**,** 1107-18.

ZHANG, Q., ZENG, L. P., ZHOU, P., IRVING, A. T., LI, S., SHI, Z. L. & WANG, L. F. 2017. IFNAR2-dependent gene expression profile induced by IFN-alpha in Pteropus alecto bat cells and impact of IFNAR2 knockout on virus infection. *PLoS One,* 12**,** e0182866.